Streamer Branching and Spectroscopic Characteristics of Surface Discharge on Water under Different Pulsed Voltages

Tomohiro Furusato, *Member, IEEE*, Takahiro Sadamatsu, Yoshinobu Matsuda and Takahiko Yamashita, *Member, IEEE*

***Abstract*— Complexity of branching pattern and OH production of water surface discharges were investigated by comparing nanosecond and microsecond water surface discharges that were defined as NWSD and MWSD, respectively. Experimental and analyzed results between NWSD and MWSD under comparable maximum discharge length l_d are summarized as follows: 1) NWSD showed the greatest complexity of branching pattern by fractal analysis; 2) electron density of NWSD was approximately two times greater than MWSD and both orders were 10^{-17} cm^{-3}; 3) emission intensity of OH (A-X) from MWSD was greater than NWSD; 4) rotational temperature of NWSD was almost constant around 1000 K irrespective of l_d and rotational temperature of MWSD increased with increasing l_d ranging from 2000 to 4000 K. It was found that the complexity of discharge pattern on water may be affected by the field intensity at water/air boundary. OH production was presumed to be caused by thermal dissociation in this experimental condition.**

***Index Terms*— Surface discharge on water, nanosecond pulsed discharge, streamer, advanced oxidation processes, fractal analysis**

I. Introduction

THE OH radicals generated via such as decomposition processes of ozone or hydrogen peroxide are effective for degradation of the persistent substance, which is so called advanced oxidation processes (AOPs). Other generation methods of OH radical in water have been investigated using ultraviolet degradation of hydrogen peroxide [1], photocatalyst [1], Fenton reaction [2], microbubble [3], electrolyzation [4], ultrasound [5] and radiation [6].

Recently, the discharge plasma that is able to generate the OH radicals directly from the H_2O molecules has been focused [7], [8]. The surface discharge generates OH radical in water via various chemical reactions at the gas-liquid interface. Thus far, the pulsed surface discharge on water was studied with several pulse widths of the applied voltage on the order of a few hundred to thousand nanoseconds [8]-[11]. Generally, the heating of discharge channel is suppressed by shortening the pulse width of voltage. The additional chemical reaction due to heating of discharge channel causes adverse effects on the efficient generation of radicals. However, the relation between the pulse width of voltage and the surface discharge on water has not drawn attention.

The complexity of discharge pattern that relates the number of discharge tip is of importance in the relatively evaluating the active site of radical formation. Detailed fractal analysis of discharge branching patterns on solid insulator has been examined [12]. In addition, H. Sakaguchi *et al*. simulated surface discharge patterns using a two-dimensional circuit model composed of capacitors and resistors whose capacitors were connected in parallel of the node of delta connection of resistors [13]. The simulation results show that the fractal dimension increases with increasing capacitance, which supports the reference [12]. The modeling of solid insulator is simple, however, the branching phenomena of surface discharge on water is not simple due to difficulty in modeling the interaction between the discharge and water.

This paper describes the complexity of discharge patterns on water with different pulse width of voltage using fractal analysis. To discuss the branching mechanism, we assume an equation of field intensity at water/air boundary. In addition, the difference of OH production and plasma behavior between different pulsed surface discharges were discussed by analyzing spectroscopic measurements.

II. Experimental Setup and Procedure

A. Experimental Setup

Two pulsed power generators were used to investigate the effect of the generator characteristics on streamer branching and plasma behavior. Blumlein line and a capacitor discharge circuit are shown in Fig. 1 (a) and (b), respectively. Tungsten was adopted as the needle electrode material. The cylindrical reactor was filled with the tap water (conductivity is 140 μS/m). The gap distance between the needle tip and the water surface was set at approximately 1 mm. A reflecting mirror tilted at 45 degrees to the ground was set above the cylindrical reactor to take images of the surface discharge by a digital CMOS camera (D610, Nikon). A carbon plate (thickness: 2 mm) was put on a grounded plate electrode to prevent the light reflection from the plate electrode. The water depth was set at 8 mm. The applied voltage and current were measured using a high voltage probe (HV-P30, IWATSU ELECTRIC Co., Ltd.) and a current

The manuscript was submitted in August 2016 “This work was partially supported by JSPS KAKENHI Grant-in-Aid for Scientific Research (C) Grant Number 16K06231”.

T. Furusato, T. Sadamatsu, Y. Matsuda and T. Yamashita are with the Graduate School of Engineering, Nagasaki University, Nagasaki 852-8521, Japan (t-furusato@nagasaki-u.ac.jp).

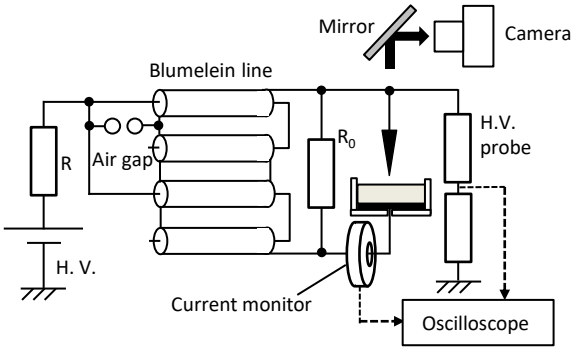

(a) Blumlein line.

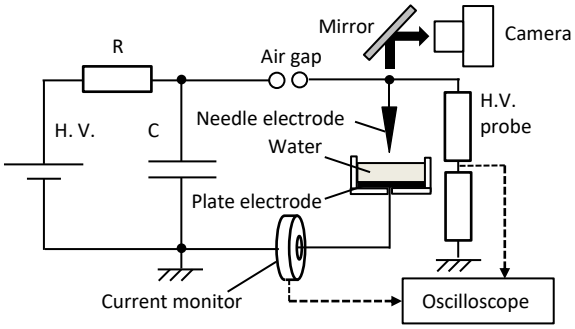

(b) Capacitor discharge circuit.

Fig. 1. Schematic diagrams of experimental setup.

monitor (Model 4100, Pearson Electronics), respectively. Waveforms were measured by an oscilloscope (DPO4104B-L, Tektronix Inc.). A CCD multi-channel spectrometer (Glacier X, B&W Tek Inc.) was used for spectroscopic measurements. A radiance calibration of the spectrometer was done in advance. Optical emission spectra were observed at just below the needle electrode.

B. Fractal Analysis

Fractal analysis of surface discharge pattern was performed by a general box counting method. For analyzing the discharge propagation patterns, computer processing was carried out to enhance the weak emission at the discharge tip. Discharge channels of the computer processed images were traced using the same thickness line in order to neglect thickness differences of discharge channel between the discharge stem and tip.

The following processes were carried out to estimate fractal dimension D of the surface discharge: 1) traced images were divided into several boxes of size r; 2) the number of boxes covering surface discharge was set as $N(r)$. The relation between $N(r)$ and r can be written as follows:

$$N(r) = r^{-D} \tag{1}$$

$$D = -\frac{\log N(r)}{\log r}. \tag{2}$$

Strong linearity of (2) provides an accurate D. Thus, the linearity was confirmed by the coefficient of determination R^2. Analyzed images show the strong linearity when R^2 is close to 1. The equation of R^2 from a regression analysis is as follows:

$$R^2 = 1 - \frac{S_e}{S_c}, \quad 0 < R^2 < 1, \tag{3}$$

where S_e is the sum of square error, S_c is the deviation of the sum of square of $\log N(r)$ and R is the coefficient of correlation.

C. Plasma Temperature Estimation

Generally, non-thermal plasma is characterized by different temperatures: electron temperature (T_e), vibrational temperature (T_{vib}), rotational temperature (T_{rot}) and translational temperature (T_{trans}). In the pulsed discharge under the atmospheric pressure, however, the condition $T_{gas} \sim T_{rot} \sim T_{rans} < T_{vib}$ is considered to hold because of the fast relaxation between rotation-to-rotation and rotation-to-translation of N_2 molecules [15]. Thus, the N_2 second positive system band (electron level; $C^3\Pi_u \rightarrow B^3\Pi_g$, vibrational level; $v' = 0 \rightarrow v'' = 0$) is used to estimate T_{rot} ($\sim T_{gas}$). The coefficients with intensity calculation of triplet systems of N_2 second positive system band are based on literatures [16], [17]. Preliminarily, the asymmetry intensity distribution due to instrumental effect of the spectrometer was measured by a He-Ne laser (632.8 nm). Phillips apparatus function is a reasonable approximation of broadening the asymmetry intensity distribution [18]. The broadening width was taken into account on the theoretical intensity calculation. The accidental error between calculation and measurement were minimized by a least-square approach.

III. RESULTS

Two kinds of pulsed power generators including Blumlein line and capacitor circuit are examined to elucidate the effects of voltage peak and pulse width of voltage on the propagation characteristics of surface discharge on water with comparable maximum discharge length l_d.

A. Discharge Images and Voltage and Current Waveforms

Images of surface discharge on water generated by Blumlein line and capacitor circuit are shown in Figs. 2(a-1) and 2(b-1), respectively. The each l_d of Figs. 2(a-1) and 2(b-1) is approximately 23 mm. The emission intensity was enhanced as

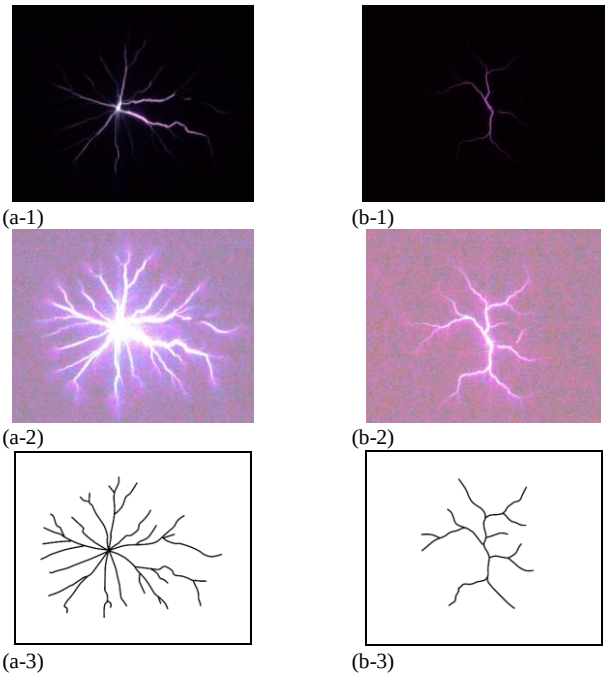

Fig. 2. Typical images of surface discharge on water at l_d = 23 mm: (a-1) Blumlein line, (b-1) capacitor circuit, (a-2) and (b-2) the corresponding computer processed images, (a-3) and (b-3) the corresponding traced images.

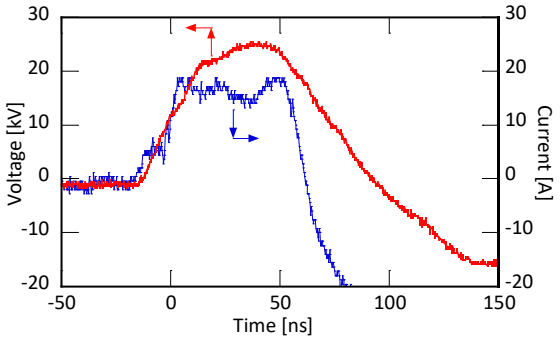

(a) Blumlein line.

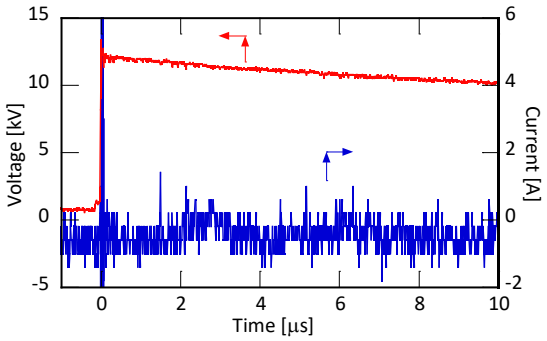

(b) Capacitor discharge circuit.

Fig. 3. Voltage and current waveforms at l_d = 23 mm.

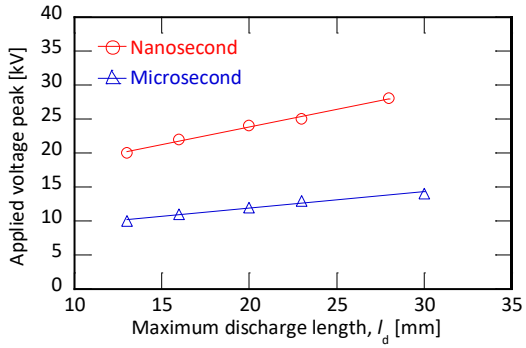

Fig. 4. Applied voltage peak as a function of maximum discharge length.

shown in Figs. 2(a-2) and 2(b-2) due to the weak emission of original images. The traced images for fractal analysis are indicated in Figs. 2(a-3) and 2(b-3). The voltage and current waveforms corresponding to Figs. 2(a-1) and 2(b-1) are shown in Figs. 3(a) and 3(b). Here, surface discharges generated by Blumlein line and capacitor circuit are defined as nanosecond water surface discharge (NWSD) and microsecond surface discharge (MWSD), respectively. The voltage peak and pulse width of NWSD under comparable l_d = 23 mm are 1.7 and 0.001 times greater than that of MWSD, respectively. The applied voltage peak was measured as a function of the l_d, as shown in Fig. 4. The ratio of the l_d to the applied voltage peak on the NWSD and MWSD are 1.96 and 4.17 mm/kV, respectively. In the case of NWSD, the discharge propagation is limited owing to the small value of the pulse width of the applied voltage. The difference in the propagation ratio in Fig. 4 indicates the additional effect of the pulse width of voltage.

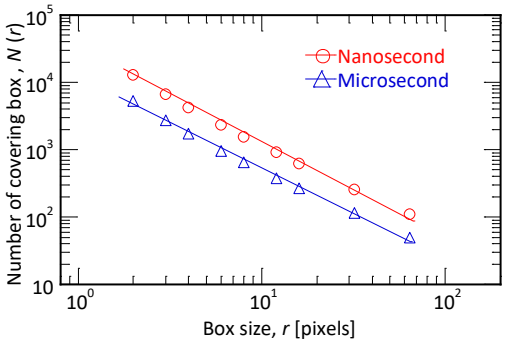

Fig. 5. Number of covering box versus box size with different pulsed discharges.

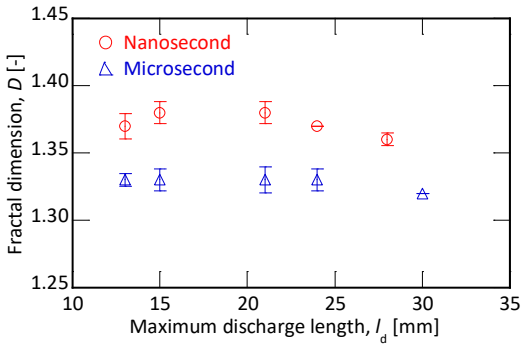

Fig. 6. Fractal dimension as a function of maximum discharge length.

B. Fractal Analysis of Discharge Patterns

Fractal analysis of Figs. 2(a-3) and 2(b-3) are performed to verify the amount of branching. The result is shown in Fig. 5. The value of negative slope corresponds to the fractal dimension D. The coefficient of determination R^2 of NWSD and MWSD are 0.997 and 0.996, indicating strong linearity because R^2 is illimitably close to 1. Strong linearity displayed by the regression line means that the treated images of surface discharge have a fractal nature. The value of D on NWSD and MWSD are 1.37 and 1.33, respectively. The higher D means much branching of discharge. Furthermore, the much branching of NWSD is also found that the number of covering box $N(r)$ with NWSD is greater than MWSD in spite of the both subequal l_d (see Fig. 5). The D was calculated as a function of the l_d, as shown in Fig. 6. The value of D on NWSD is higher than that of MWSD irrespective of l_d. Therefore, the value of D is also independent of the peak value of voltage in comparison with Fig. 4.

C. Spectroscopic Measurement

Optical emission spectra of NWSD and MWSD are shown in Fig. 7. They are normalized by the intensity of N_2 (0-0) peak. N_2 (C-B) and OH (A-X) at 310 nm are observed in the range from 280 to 420 nm. OH (A) is produced by a large number of reactions. OH (A) production by dissociative excitation from H_2O is supposed as follows [19]:

$$H_2O(X) + e \rightarrow OH(A) + H(n=1) + e. \quad (4)$$

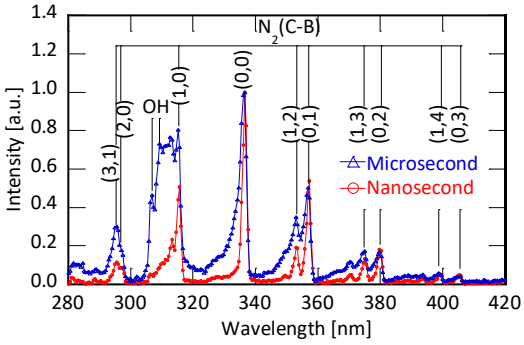

Fig. 7. Optical emission spectra of different pulsed discharge on water.

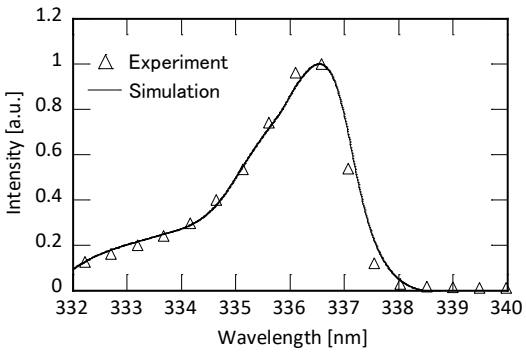

Fig. 8. Measurement point and simulation spectra of microsecond pulsed discharge at N_2 second positive system (0-0).

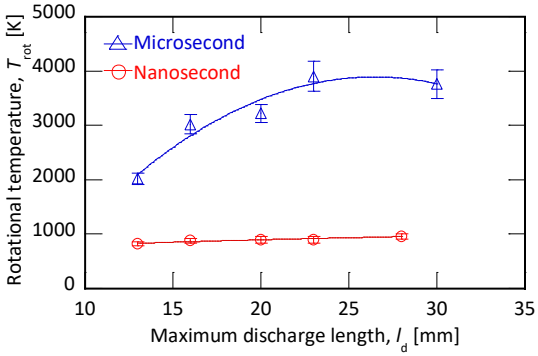

Fig. 9. Rotational temperature versus maximum discharge length.

In addition, OH (A) production by metastable N_2 (A) (vibrational revel $v' \geqq 21$) was reported under N_2/H_2O mixture [20]:

$$H_2O(X) + N_2(A) \rightarrow OH(A) + H(n=1) + N_2(X). \quad (5)$$

However, according to [21], almost N_2 (A) are quenched by O_2 under atmospheric air. Consequently, OH (A) production by N_2 (A) can be negligible in this study. Secondary excitation reaction from OH (X) to OH (A) (4 eV) plays a significant role in the production of OH (A) owing to low dissociation energy of water bonding O-OH (5.1 eV) [22]. The following reactions of OH (X) productions are supposed by some literatures [22]-[24]:

$$H_2O(X) + e \rightarrow OH(X) + H(n=1) + e \quad (6)$$
$$H_2O(X) + O(^1D) \rightarrow 2OH(X) \quad (7)$$
$$H_2O + e \rightarrow OH(X) + H^- \quad (8)$$
$$e + H_2O^+ \rightarrow OH(X) + H \quad (9)$$
$$e + H_3O^+ \rightarrow OH(X) + H_2 + e. \quad (10)$$

The emission intensity of OH (A-X) with P and R branches around 310 nm of MWSD is obviously greater than that of NWSD. D. Yang *et al*. reported that the emission intensity of OH (A-X) decreased with increasing the gap distance of electrode with a homogeneous dielectric barrier nanosecond pulsed discharge at atmospheric humid air [21]. Meanwhile, the intensity of OH (A-X) increased with increasing applied voltage under same gap distance. Their results indicate the intensity of OH (A-X) depends on the reduced field intensity (E/N). Although the applied voltage of NWSD is approximately two times greater than MWSD (see Fig. 4), the intensity of OH (A-X) is independent of the E/N at the needle electrode. The cause of the difference of OH intensity will discuss in the Section IV-C.

D. Plasma Temperature Characteristics

To estimate the gas temperature of plasma, the simulation spectra is fitted to the measurement one of N_2 (C-B, 0-0) by a least-square approach as shown in Fig. 8. The simulation spectra is a function of the T_{rot} temperature. The detailed simulation method was explained in Section II-C. Characteristic of T_{rot} is shown in Fig. 9 as a function of l_d. The T_{rot} of NWSD is almost constant irrespective of the l_d. On the other hand, T_{rot} of MWSD increased with increasing l_d.

IV. Discussion

A. Streamer Branching on Water Surface

As mentioned in section III-B, the high-complexity discharge pattern of NWSD was indicated by a fractal analysis. Here, the streamer branching on water is discussed based on the electric field along the water surface and the initial electron. The electric field is rearranged at the moment when a discharge bridges the air gap between needle and water. The current flow in the water affects the electric field along the water surface. The current value of NWSD is one order larger than MWSD as shown in Fig. 3. When we assume the conduction current flows radially in water, the field intensity E in water at the arbitrary distance d from the flowing current point can be expressed based on an electromagnetic theory as follows:

$$E = \frac{\rho I}{2\pi d^2}, \quad (11)$$

where ρ is resistivity of water and I is conduction current in water. It can be assumed that the E is almost same at the boundary between water and air. According to (11), the field intensity is determined by the value of I because the ρ is same in the cases of NWSD and MWSD.

Field intensity at the discharge tip has an influence on the generation of initial electron around the tip. According to [25], [26], the electron detachment from the O_2^- and $O_2^-(H_2O)$ cluster may be possible dominant mechanism in humid air since the probability of electron production with the natural ionizing

from cosmic ray or natural phenomena is negligible small due to short sustaining period of the voltage within a few tens of microseconds. It is supposed that initial electrons are rich at the tip of NWSD because the detachment lifetime of negative ions is a function of E/N [25].

A. Kulikovsky simulated a propagation of positive streamer in atmospheric air by two-dimensional modeling with process of photoionization [27]. The results showed that the streamer branching appeared when the potential at the anode tip increased. As stated above, NWSD requires approximately two times higher voltage to form the identical l_d of MWSD, as shown in Fig. 4. Consequently, it is reasonable for the NWSD to propagate with a large number of branches due to the high potential of the streamer tip.

B. Electron Density and Discharge Phase Transition

The spectrum line profile of H_α is shown in Fig. 10. The intensity are normalized by intensity of N_2 (0-0) peak. The full width of half maximum (FWHM) of NWSD is greater than that of MWSD. Generally, H_α is mainly broadened by the Stark broadening that correlates with the electron density. The electron density N_e in cm^{-3} is determined by following equation [28]:

$$N_e = 8.02\times10^{12}\left(\frac{\lambda_{1/2}}{\alpha_{1/2}}\right)^{3/2}, \qquad (12)$$

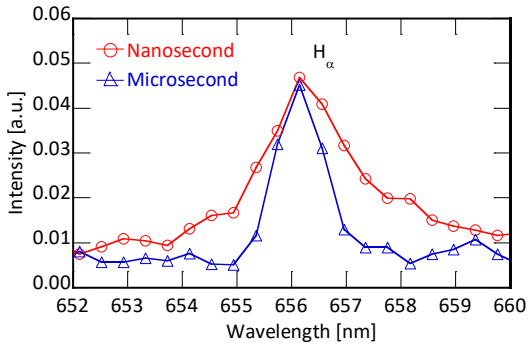

Fig. 10. H_α spectra at different pulsed discharges on water. The intensities are normalized by intensity of N_2 (0-0) peak.

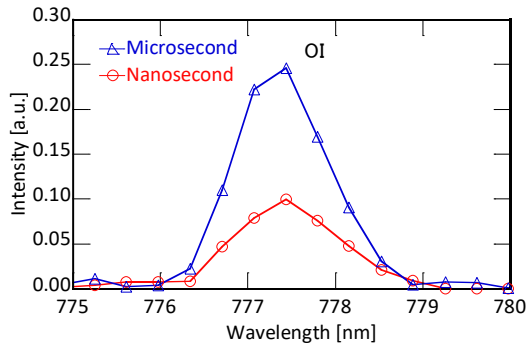

Fig. 11. OI spectra at different pulsed discharges on water. The intensities are normalized by intensity of N_2 (0-0) peak.

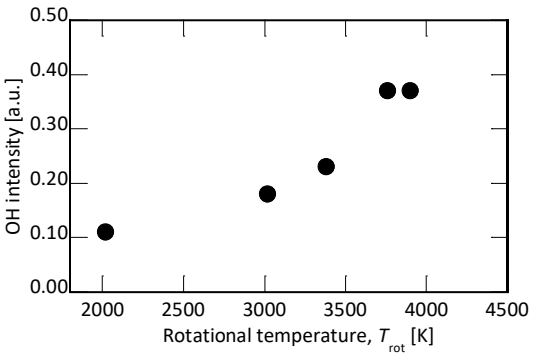

Fig. 12. OH intensity with microsecond pulsed discharge (R branch, 307 nm) versus rotational temperature.

where $\lambda_{1/2}$ is FWHM of Stark broadening in angstroms and $\alpha_{1/2}$ is half width of reduced Stark broadening in angstroms. The $\alpha_{1/2}$ is a function of the electron density and temperature [29]. Stark broadening can be supposed Lorentzian profile. Convolution of Lorentzian and instrumental function was carried out to fit the measured H_α. Estimated N_e with NWSD and MWSD were approximately 2×10^{-17} and 1×10^{-17} cm^{-3}, respectively. A large number of N_e in NWSD may be supposed by a large number of streamer tips and the small diameter of the discharge channel.

Fig. 11 shows the emission from $O(^5P)$ species at 777 nm. The intensity are normalized by the intensity of N_2 (0-0) peak. The intensity of MWSD was greater than that of NWSD. M. Janda *et al*. supposed that the phase transition of streamer to spark discharge in atmospheric air by emission intensity of $O(^5P)$ as indicated in the following steps [30]:

$e + N_2(X) \rightarrow e + N_2(C)$	streamer phase	(13)
$N_2(C) + O_2 \rightarrow N_2(X) + 2O(^3P)$	transition phase	(14)
$e + O(^3P) \rightarrow e + O(^5P)$	spark phase.	(15)

As the result of Fig. 11, the discharge phase of MWSD may transit close to the spark phase due to its large number of $O(^5P)$ population. In addition, as stated in Section III-D, MWSD are also characterized by the high T_{rot} (see Fig. 9).

C. OH Production by Thermal Dissociation

As shown in Fig. 7, OH (A-X) intensity from MWSD was greater than that from NWSD. The T_{rot} may affect the OH production due to a profound difference of T_{rot} between NWSD and MWSD (see Fig. 9). P. Bruggeman *et al*. investigated gas temperature dependence of production reaction rates of OH for 1 eV plasma with following thermal dissociation [24]:

$$H_2O + H_2O \rightarrow OH(X) + H + H_2O. \qquad (14)$$

According to their results, the production rate of OH increases with increasing gas temperature unless the plasma is LTE condition. T_{rot} dependence of the intensity of OH (R branch, 307 nm) with MWSD is shown in Fig. 12. T_{rot} may be effective for the increase of OH intensity for MWSD, because significant gas heating is expected for MWSD compared with NWSD.

V. Concluding Remarks

This study deals with the complexity of discharge branching pattern on water surface discharge and OH production to compare NWSD and MWSD. The complexity is quantitatively assessed by a fractal dimension D. To elucidate the differences of plasma behavior between NWSD and MWSD, electron density and T_{rot} were estimated by analyzing H_α and N_2 second positive system, respectively. The experiments are carried out in the range within similar l_d between NWSD and MWSD. The results are summarized as follows.

1) The D of discharge pattern with NWSD was greater than MWSD irrespective of l_d. An assumed equation indicates that the field intensity at water/air boundary depends on the current. The current with NWSD was about one order greater than MWSD. The reason of large D of NWSD is believed that the large field intensity at water surface produces a large number of initial electrons by electron detachment from O_2^- and $O_2^-(H_2O)$.
2) Electron density with NWSD was about two times greater than MWSD. On the other hand, the emission intensity of O (^{5}P) at 777 nm with MWSD is greater than NWSD. It is inferred that the MWSD may transit close to spark phase.
3) Emission intensity of OH (A-X) and T_{rot} of MWSD is greater than NWSD. The results suggest that the thermal dissociation plays a significant role in emission intensity of OH (A-X).

Acknowledgments

This work was partially supported by JSPS KAKENHI Grant-in-Aid for Scientific Research (C) Grant Number 16K06231. We would like to thank Mr. Hiroyuki Koreeda, technician, for his assistance in the experiments.

References

[1] R. Andreozzi, L. Campanella, B. Fraysse, J. Garric, A. Gonnella, R. Lo Giudice, "Effects of advanced oxidation processes (AOPs) on the toxicity of a mixture of pharmaceuticals," *Water Science and Technology*, vol. 50, no. 5, pp. 23-28, Feb. 2004.

[2] R. V. Lloyd, P. M. Hanna, and R. P. Mason, "The origin of the hydroxyl radical oxygen in the Fenton reaction," *Free Radical Biology and Medicine*, vol. 22, no. 5, pp. 885-888, Feb. 1997.

[3] M. Takahashi, K. Chiba, and P. Li, "Free-Radical Generation from Collapsing Microbubbles in the Absence of a Dynamic Stimulus," *J. Phys. Chem. B*, vol. 111, no. 6, pp. 1343-1347, Feb. 2007.

[4] E. Fockedey, and A. V. Lierde, "Coupling of anodic and cathodic reactions for phenol electro-oxidation using three-dimensional electrodes," *Water Res.*, vol. 36, no. 16, pp. 4169-4175, Sep. 2002.

[5] A. K. Jana, and S. N. Chatterjee, "Estimation of hydroxyl free radicals produced by ultrasound in Fricke solution used as a chemical dosimeter," *Ultrasonics Sonochemistry*, vol. 2, no. 2, pp. S87-S91, Jan. 1995.

[6] M. A. Rauf, and S. S. Ashraf, "Radiation induced degradation of dyes - An overview," *Journal of Hazardous Materials*, vol. 166, no. 1, pp. 6-16, Jul. 2009.

[7] B. R. Locke, M. Sato, P. Sunka, M. R. Hoffmann, and J.-S. Chang, "Electrohydraulic Discharge and Nonthermal Plasma for Water Treatment," *Ind. Eng. Chem. Res.*, vol. 45, no3, pp. 882-905, Feb. 2006.

[8] P. Lukes, E. Dolezalova, I. Sisrova, and M. Clupek, "Aqueous-phase chemistry and bactericidal effects from an air discharge plasma in contact with water: evidence for the formation of peroxynitrite through a pseudo-second-order post-discharge reaction of H_2O_2 and HNO_2," *Plasma Sources Sci. Technol.*, vol. 23, no. 1, pp. 015019-1 – 015019- 15, Feb. 2014.

[9] S. Kanazawa, H. Kawano, S. Watanabe, T. Furuki, S. Akamine, R. Ichiki, T. Ohkubo, M. Kocik and J. Mizeraczyk, "Observation of OH radicals produced by pulsed discharges on the surface of a liquid," *Plasma Sources Sci. Technol.*, vol. 20, no. 3, 034010-1 – 034010-8, Jun. 2011.

[10] K. Yoshihara, Ruma, S. H. R. Hosseini, T. Sakugawa, and H. Akiyama, "Study of Hydrogen Peroxide Generation by Water Surface Discharge," *IEEE Trans. Plasma Sci.*, vol. 42, no. 10, pp. 3226-3230, Oct. 2014.

[11] S. Kanazawa, S. Geng, T. Okawa, S. Akamine and R. Ichiki, "Improvement of Surfactant Decomposition by Superpositon of Pulsed Discharge on the Water and Ozone Injection," *Int. J. PEST*, vol. 7, no. 1, pp. 21-25, Mar. 2013.

[12] L. Kebbabi and A. Beroual, "Fractal analysis of creeping discharge patterns propagating at solid/liquid interfaces: influence of the nature and geometry of solid insulators," *J. Phys. D: Appl. Phys.*, vol. 39, no. 1, pp. 177-183, Jan. 2006.

[13] H. Sakaguchi, and S. M. Kourkouss, "Branching Patterns and Stepped Leaders in an Electric-Circuit Model for Creeping Discharge," *J. Phys. Soc. Jpn.*, vol. 79, no. 6, 064802-1 – 064802-5, Jun. 2010.

[14] M. Sato, T. Tokutake, T. Oshima, and T. Sugiarto, "Aqueous Phenol Decomposition by Pulsed Discharges on the Water Surface," *IEEE Trans. Ind. Appl.*, vol. 44, no. 5, pp. 1397-1402, Sep. 2008.

[15] D. Staack, B. Farouk, A. Gutsol and A. Fridman, "Spectroscopic studies and rotational and vibrational temperature measurements of atmospheric pressure normal glow plasma discharges in air," *Plasma Sources Sci. Technol.*, vol. 16, no. 4, pp. 818-827, Jun. 2006.

[16] G. Hartmann and P. C. Johnson, "Measurements of relative transition probabilities and the variation of the electronic transition moment for N_2 $C^3\Pi_u$-$B^3\Pi_g$ second positive system," *J. Phys. B, Atomic Molecular Phys.*, vol. 11, no. 9, pp. 1597–1612, 1978.

[17] G. Herzberg, "Molecular Spectra and Molecular Structure I. Spectra of Diatomic Molecules," *D. Van Nostrand Company Inc.*, New York, p. 552, 1950.

[18] D. M. Phillips, "Determination of gas temperature from unresolved bands in the spectrum from a nitrogen discharge," *J. Phys. D, Appl. Phys.*, vol. 9, no. 3, p. 507, 1975.

[19] C. Beenakker, F. Deheer, H. Krop, and G. Mohlmann, "Dissociative excitation of water b electron impact," *Chem. Phys.*, vol. 6, no. 3, pp. 445-454, Dec. 1974.

[20] F. Tochikubo and T. Teich, "Optical Emission from a Pulsed Corona Discharge and Its Associated Reactions," *Jpn. J. Appl. Phys.*, vol. 39, no. 3A, pp. 1343-1350, 2000.

[21] D. Yang, Y. Yang, S. Li, D. Nie, S. Zhang and W. Wang, "A homogeneous dielectric barrier discharge plasma excited by a bipolar nanosecond pulse in nitrogen and air," *Plasma Sources Sci. Technol.*, vol. 21, no. 21, pp. 035004-1 – 035004-9, Jun. 2006.

[22] B. Benstaali, P. Boubert, B. Cheron, A. Addou and J. Brisset, "Density and Rotational Temperature Measurements of the OH and NO Radicals Produced by a Gliding Arc in Humid Air," *Plasma Chem. and Plasma Processing*, vol. 22, no. 4, pp. 553–571, Dec. 2012.

[23] B. Sun, S. Kunitomo, and C. Igarashi, "Characteristics of ultraviolet light and radicals formed by pulsed discharge in water," *J. Phys. D, Appl. Phys.*, vol. 39, no. 17, pp. 3814-3820, Aug. 2006.

[24] P. Bruggeman, and D. Schram, "On OH production in water containing atmospheric pressure plasmas," *Plasma Sources Sci. Technol.*, vol. 19, pp. 045025-1 – 045025-9, Jul. 2010.

[25] S. Badaloni and I. Gallimberti, "Basic Data of Air Discharges," *Universita' di Padova Report*, Upee-72/05, Jun. 1972.

[26] N. Harid, and R. Waters, "Statistical study of impulse corona inception parameters on line conductors," *IEE Proc. A*, vol. 138, no. 3, pp. 161 – 168, May 1991.

[27] A. Kulikovsky, "The role of photoionization in positive streamer dynamics," *J. Phys. D: Appl. Phys.*, vol. 33, no. 12, pp. 1514 – 1524, Mar. 2000.

[28] J. Ashkenazy, R. Kipper, and M. Caner, "Spectroscopic measurements of electron density of capillary plasma based on Stark broadening of hydrogen lines," *Phys. Rev. A*, vol. 43, no. 10, pp. 5568 – 5574, May 1991.

[29] H. R. Griem, "Spectral Line Broadening by Plasmas," *Academic Press New York and London*, 1974.

[30] M. Janda, Z. Machala, A. Niklova, and V. Martisovits, "The streamer-to-spark transition in a transient spark: a dc-driven nanosecond-pulsed discharge in atmospheric air," *Plasma Sources Sci. Technol.*, vol. 21, pp. 045006-1 – 045006-9, Jun. 2012.

Tomohiro Furusato (S'13-M'14) was born in Kagoshima, Japan, in 1988. He received the B. E., M. E., and Ph. D. degrees from Kumamoto University, Kumamoto Japan, in 2011, 2012, and 2014, respectively. He was with the Japan Society for the Promotion of Science, Kumamoto University, from 2013 to 2014, as a Research Fellow. Since 2014, he has been an Assistant Professor with the Graduate School of Engineering, Nagasaki University, Nagasaki, Japan. His research interests are pulsed-power, surface discharge, and discharge phenomena in supercritical fluids.

Takahiro Sadamatsu was born in Nagasaki, Japan, in 1992. He received B. E. degree in 2015 from Nagasaki University, Nagasaki, Japan, where he is currently working toward the M. E. degree. His current research interest is surface discharge phenomena on water.

Yoshinobu Matsuda was born in Miyazaki, Japan, in 1960. He received B. S. degree from Kyoto University, Kyoto Japan in 1982, and M. E. and Ph. D. degrees from Kyushu University, Fukuoka Japan in 1984 and 1987, respectively. After working as an Assistant Researcher with the Graduate School of Science and Engineering, Kyushu University from 1987 to 1988, he joined the Department of Electrical and Electronic engineering, Nagasaki University as a Lecturer. Since 1990, he has been an Assistant Professor with the Graduate School of Engineering, Nagasaki University, Nagasaki, Japan. His research interests are plasma diagnostics, plasma surface interaction, and engineering application of plasmas, plasma processing of thin films in particular.

Takahiko Yamashita (M'00) was born in 1957 at Fukuoka in Japan. He received the B. E., M. E. and D. E. degrees from Kyushu University in 1980, 1982 and 1985, respectively. He has been working in Nagasaki University, Nagasaki, Japan since 1985. He is a professor of Graduate School of Engineering and a Vice President of Nagasaki University. He is a senior member of Institute of Electrical Engineers Japan.